INTERNATIONAL JOURNAL FOR NUMERICAL METHODS IN FLUIDS
Int. J. Numer. Meth. Fluids 2001; **37**: 525–540 (DOI: 10.1002/fld.185)

Numerical analysis of interfacial two-dimensional Stokes flow with discontinuous viscosity and variable surface tension

Zhilin Li[a,*,1] and Sharon R. Lubkin[a,b,2]

[a] *Center for Research in Scientific Computation and Department of Mathematics, North Carolina State University, Raleigh, NC, U.S.A.*
[b] *Biomathematics Program, North Carolina State University, Raleigh, NC, U.S.A.*

SUMMARY

A fluid model of the incompressible Stokes equations in two space dimensions is used to simulate the motion of a droplet boundary separating two fluids with unequal viscosity and variable surface tension. Our theoretical analysis leads to decoupled jump conditions that are used in constructing the numerical algorithm. Numerical results agree with others in the literature and include some new findings that may apply to processes similar to cell cleavage. The method developed here accurately preserves area for our test problems. Some interesting observations are obtained with different choices of the parameters. Copyright © 2001 John Wiley & Sons, Ltd.

KEY WORDS: discontinuous and non-smooth solution; immersed interface method; interface; jump condition; Stokes equation; variable surface tension

1. INTRODUCTION

The Stokes equations have been widely used to simulate the deformation and cleavage of fluid droplets, and the fluid droplets have been used as a model for the deformation and cleavage of cells, e.g. References [1–3]. *In vivo* or *in vitro*, cells live surrounded by a medium, which can be mechanically significant, yet most biomechanical analyses of cell and tissue deformations stop at the cell membrane or basal lamina. In this paper, we consider the fluids inside and outside an evolving interface, where the two fluids may be of unequal viscosity. Let $\Omega = \Omega^- \cup \Omega^+ \cup \Gamma$ be a bounded domain, where Ω^- is the inside fluid, Ω^+ is the outside fluid, and Γ is the interface between them, which is closed; see Figure 1 for an illustration.

* Correspondence to: Center for Research in Scientific Computation, North Carolina State University, Raleigh, NC 27695-8205, U.S.A.
[1] E-mail: zhilin@math.ncsu.edu
[2] E-mail: lubkin@eos.ncsu.edu

Received 29 January 1999
Revised 24 October 2000

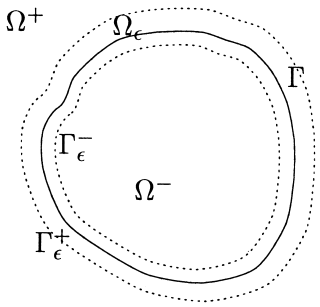

Figure 1. A diagram of the geometry discussed in this paper as used for the derivation of jump relations.

We use the following Stokes equation with a periodic boundary condition to study the motion of the fluids inside and outside of a droplet:

$$\nabla p = \mu \Delta \mathbf{u}, \qquad (x, y) \in \Omega - \Gamma \tag{1.1}$$

$$\nabla \cdot \mathbf{u} = \mathbf{0}, \qquad (x, y) \in \Omega \tag{1.2}$$

$$\text{Periodic BC for } \mathbf{u} \text{ and } p \tag{1.3}$$

where $\mathbf{u} = (u, v)$ is the velocity vector, p is the pressure, μ is the viscosity, defined as piecewise constant, with

$$\mu = \begin{cases} \mu^- & \text{if } (x, y) \in \Omega^- \\ \mu^+ & \text{if } (x, y) \in \Omega^+ \end{cases} \tag{1.4}$$

The periodic boundary condition is justified since for many biological problems, we assume that the far-field conditions are unimportant; e.g. see References [4,5] and the references therein. Across the interface, there are the jump conditions, see e.g. [1,6,7]

$$[p - 2\mu(\nabla u \cdot \mathbf{n}, \nabla v \cdot \mathbf{n}) \cdot \mathbf{n}] = \gamma(s)\kappa \tag{1.5}$$

$$[\mu(\nabla u \cdot \mathbf{n}, \nabla v \cdot \mathbf{n})] \cdot \mathbf{t} + \mu(\nabla u \cdot \mathbf{t}, \nabla v \cdot \mathbf{t}) \cdot \mathbf{n}] = -\frac{\partial \gamma(s)}{\partial \mathbf{t}} \tag{1.6}$$

where s is the counterclockwise arc-length parameterization along the interface, $\mathbf{n}$ and $\mathbf{t}$ are the unit outwards normal and counter-clockwise tangent directions of the interface, κ is the curvature

$$\frac{\partial \gamma(s)}{\partial \mathbf{t}} = \nabla \gamma(s) \cdot \mathbf{t}$$

is the derivative of $\gamma(s)$ along the tangential direction, the jump $[\cdot]$ is defined as the difference between the limiting value from outside the cell boundary and that from the inside, and $\gamma(s)$ is the surface tension, which may be modeled by a separate equation [1,2]. In this paper, we allow surface tension to be constant or a simple function defined on the surface of the cell. The surface tension is the main driving force for the cell deformation. The interface has the same velocity as the fluids surrounding it

$$\frac{\partial \Gamma}{\partial t} = \mathbf{u} \tag{1.7}$$

hence mass inside or outside the interface is conserved. We assume that the flow is isothermal, therefore the velocity is continuous across the interface [8].

Almost all the numerical simulations for viscous droplet dynamics with a free boundary are based on a boundary integral method; see for example, [9,10] and some others. Few examples can be found in the literature that use the finite element method [6] or finite difference method to solve the problems because of the prohibitive computational cost to solve the problem in the entire domain when the jump in the viscosity is large. However, when the viscosity is continuous, the problem can be solved easily with the finite difference method (see References [11,12] and others). In this paper, we use a finite difference method based on a fast Poisson solver to solve the two-fluid moving interface problem. One of the advantages of this approach is that we are able to obtain the velocity and pressure in the entire domain without sacrificing the speed of the simulation. The approach described here is not tied to a boundary integral equation, making it potentially useful for constructing some desired force to control the shape of the moving interface, even if a boundary integral equation is not available or difficult to derive.

Outside and inside the domain excluding the interface, Equation (1.1) can be reformulated as a sequence of three Poisson problems, one for each variable due to the incompressibility condition. For piecewise constant viscosity, applying the divergence operator to Equation (1.1) and using the incompressibility condition, we get

$$\Delta p = 0, \quad (x, y) \in \Omega - \Gamma, \qquad \text{periodic BC on } \partial\Omega \text{ for } p \tag{1.8}$$

where Δ is the Laplacian operator. Although p satisfies the Laplace equation in the domain excluding the interface Γ, it is a Poisson problem for the pressure in the entire domain since the jump conditions for the pressure correspond to single and double source distributions along the interface Γ. Once p is known, Equation (1.1) represents two independent Poisson problems for u and v respectively. However, the solutions outside and inside are not independent. A numerical algorithm that ignores the coupling relations usually lowers the accuracy especially at or near the interface. In this paper, we derive the jump conditions of the solution across the interface and use them to construct an accurate solution method.

The rest of the paper is organized as follows. In Section 2, we derive the jump conditions for Equations (1.1)–(1.3). In Section 3, we outline our numerical algorithm, which is rather straightforward once we know the jump conditions. Numerical experiments are provided and analyzed in Section 4. Some conclusions will be given in Section 5.

2. DERIVING THE JUMP CONDITIONS

Using the immersed interface method (IIM) [13–17] we can solve the three Poisson equations for u, v, and p efficiently if we know the jump conditions in the solution and in the flux. However, the jump conditions given in Equations (1.5) and (1.6) are coupled and we cannot use them directly. The approach used in [11] for the Stokes equation cannot be applied due to the discontinuity in the viscosity. Fortunately, the following theorem gives decoupled jump conditions.

Theorem 1
Let p, u, and v be the solution of Equations (1.1)–(1.3) with the jump conditions (1.5) and (1.6). If $\gamma(s)$ is smooth enough such that the solution p and $\mathbf{u}$ are *piecewisely* twice differentiable, then the following equalities hold:

$$\left[\mu \frac{\partial \mathbf{u}}{\partial \mathbf{n}}\right] = \frac{\partial \gamma(s)}{\partial \mathbf{t}} \mathbf{t} \tag{2.9}$$

$$[p] = \gamma(s)\kappa \tag{2.10}$$

$$\left[\frac{\partial p}{\partial \mathbf{n}}\right] = \frac{\partial^2 \gamma}{\partial \mathbf{t}^2} \tag{2.11}$$

where

$$\frac{\partial p}{\partial \mathbf{n}} = \nabla p \cdot \mathbf{n}$$

Note that while p and u may not be smooth—and p may not even be continuous—across the interface, it is reasonable to assume that the velocity and pressure are smooth *inside* and *outside* of the interface *excluding* the interface.

To prove the theorem, it is more convenient to use the local co-ordinates. Let (X, Y) be a point on the interface, and the unit normal and tangential directions are

$$\mathbf{n} = (\cos\theta, \sin\theta), \qquad \mathbf{t} = (-\sin\theta, \cos\theta)$$

respectively, where θ is the angle between the outward normal direction and the x-axis; see Figure 2 for an illustration. The local co-ordinates at (X, Y) then are

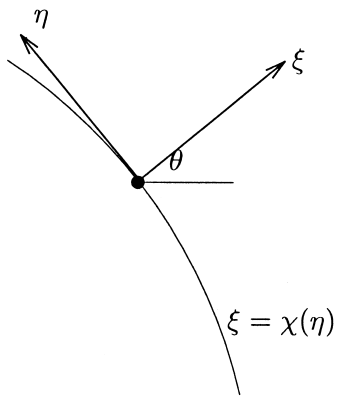

Figure 2. Local co-ordinates and geometry.

$$\xi = (x - X)\cos\theta + (y - Y)\sin\theta \tag{2.12}$$

$$\eta = -(x - X)\sin\theta + (y - Y)\cos\theta$$

We first prove the following lemma, which is needed in the proof of Theorem 1.

Lemma 1
Assume the conditions in Theorem 1 are true. Let **u** be the solution to (1.1)–(1.3). Then the following equalities are true:

$$[\mu(u_{xx} + u_{xy})] = 0, \qquad [\mu(u_{xy} + v_{yy})] = 0 \tag{2.13}$$

$$[\mu u_x \cos\theta + v_x \sin\theta] = 0, \qquad [\mu u_y \cos\theta + v_y \sin\theta] = 0 \tag{2.14}$$

Proof
In the inside and outside of the domain excluding the interface, we have

$$u_x + v_y = 0 \quad \text{and} \quad \mu(u_x + v_y) = 0$$

$$\mu(u_{xx} + v_{xy}) = 0 \quad \text{and} \quad \mu(v_{xy} + v_{yy}) = 0$$

Therefore, we can continuously extend the definitions above to everywhere inside the domain Ω and we have the equalities in (2.13).

To prove the second part, we enclose the interface with a small domain Ω_ϵ; see Figure 1 for an illustration. Let $\phi(x, y) \in C^\infty$ be a two-dimensional test function. Since $\mu(u_{xx} + v_{xy})$ and $\mu(u_{xy} + v_{yy})$ are continuous inside $\Omega(\epsilon)$ after the extension, we have

$$\mu(u_{xx}+v_{xy})=\nabla\cdot\mu\begin{bmatrix}u_x\\v_x\end{bmatrix}=0 \tag{2.15}$$

$$\mu(u_{xy}+v_{yy})=\nabla\cdot\mu\begin{bmatrix}u_y\\v_y\end{bmatrix}=0 \tag{2.16}$$

Here we have used the fact that μ is piecewise constant and

$$\mu(u_{xx}+v_{xy})=\frac{\partial}{\partial x}\left(\mu\frac{\partial v}{\partial y}\right)+\frac{\partial}{\partial x}\left(\mu\frac{\partial v}{\partial y}\right)=0$$

has continuous extension across the cell boundary. Multiply (2.15) by any test function $\phi(x, y)\in C^{\infty}(\Omega)$ and integrate over Ω_{ϵ}. From Green's theorem, we have

$$\begin{aligned}&\lim_{\epsilon\to 0}\iint_{\Omega_\epsilon}\phi\nabla\cdot\left(\mu\begin{bmatrix}u_x\\v_x\end{bmatrix}\right)\mathrm{d}x\ \mathrm{d}y\\&=\int_{\Gamma}\phi[\mu(u_x\cos\theta+v_x\sin\theta]\,\mathrm{d}s+\lim_{\epsilon\to 0}\iint_{\Omega_\epsilon}\nabla\phi\cdot\begin{bmatrix}u_x\\v_x\end{bmatrix}\mu\ \mathrm{d}x\ \mathrm{d}y\\&=\int_{\Gamma}\phi[\mu(u_x\cos\theta+v_x\sin\theta)]\,\mathrm{d}s=0\end{aligned}$$

where we have used the fact that μ, u_x, and v_x are bounded. Since ϕ is arbitrary, we conclude that

$$[\mu(u_x\cos\theta+v_x\sin\theta)]=0 \tag{2.17}$$

Similarly, we can get

$$[\mu(u_y\cos\theta+v_y\sin\theta)]=0 \tag{2.18}$$

This completes the proof of the lemma.

Proof of Theorem 1
Expressing the jump condition (1.6) in terms of the local co-ordinates, we get

$$-\sin\theta[\mu u_{\xi}]+\cos\theta[\mu v_{\xi}]+\cos\theta[\mu u_{\eta}]+\sin\theta[\mu v_{\eta}]=-\frac{\partial\gamma(s)}{\partial\mathbf{t}} \tag{2.19}$$

Expressing the jump condition $[\mu(u_x+v_y)]=0$ in terms of the local co-ordinates, we have

$$\cos\theta[\mu u_\xi] + \sin\theta[\mu v_\xi] - \sin\theta[\mu u_\eta] = 0 \tag{2.20}$$

Under the local co-ordinates, the two equalities in (2.14) are

$$\cos^2\theta[\mu u_\xi] + \sin\theta\cos\theta[\mu v_\xi] - \sin\theta\cos\theta[\mu u_\eta] - \sin^2\theta[\mu v_\eta] = 0 \tag{2.21}$$

$$\sin\theta\cos\theta[\mu u_\xi] + \sin^2\theta[\mu v_\xi] + \cos^2\theta[\mu u_\eta] + \sin\theta\cos\theta[\mu v_\eta] = 0 \tag{2.22}$$

The coefficient matrix of (2.19)–(2.22) is non-singular, and its inverse is

$$\begin{bmatrix} -\sin\theta & 0 & 2\cos^2\theta - 1 & 2\sin\theta\cos\theta \\ \cos\theta & 0 & 2\sin\theta\cos\theta & -2\cos^2\theta + 1 \\ 0 & -\sin\theta & 0 & 1 \\ 0 & \cos\theta & -1 & 0 \end{bmatrix} \tag{2.23}$$

Therefore we have proved that

$$[\mu u_\xi] = -\frac{\partial\gamma}{\partial\mathbf{t}}\sin\theta, \qquad [\mu v_\xi] = \frac{\partial\gamma}{\partial\mathbf{t}}\cos\theta$$

which is (2.9) in Theorem 1. The proof of (2.10) is straightforward if we substitute the equalities above into (1.5).

From the system of equations and the inverse of the coefficient matrix, we also conclude that

$$[\mu u_\eta] = 0, \qquad [\mu v_\eta] = 0$$

Let the interface Γ be $\xi = \chi(\eta)$ in the neighborhood of $(\xi, \eta) = (0, 0)$, which satisfies $\chi(0) = 0$, $\chi'(0) = 0$. Then $\chi''(0) = \kappa$, the curvature of the interface at (0,0). Differentiating $[\mathbf{u}_\eta] = \mathbf{0}$ along the tangential direction, we get

$$[\mu u_{\eta\eta}] = 0, \qquad [\mu v_{\eta\eta}] = 0 \tag{2.24}$$

Differentiating

$$[\mu\mathbf{u}_\xi] = \frac{\partial\gamma}{\partial\mathbf{t}}\mathbf{t}$$

along the tangential direction, we get

$$[\mu u_{\xi\eta}] = \frac{\partial^2\gamma}{\partial\mathbf{t}^2}\mathbf{t} + \kappa\frac{\partial\gamma}{\partial\mathbf{t}}\mathbf{n} \tag{2.25}$$

Expressing $[\mu(u_{xx}+v_{xy})]=0$ and $[\mu(u_{xy}+v_{yy})]=0$ in the local co-ordinates, we obtain

$$[\mu(u_{\xi\xi}\cos^2\theta-2u_{\xi\eta}\cos\theta\sin\theta+u_{\eta\eta}\sin^2\theta+v_{\xi\xi}\cos\theta\sin\theta+v_{\xi\eta}(\cos^2\theta-\sin^2\theta)-v_{\eta\eta}\cos\theta\sin\theta)]=0$$

$$[\mu(u_{\xi\xi}\cos\theta\sin\theta+u_{\xi\eta}(\cos^2\theta-\sin^2\theta)-u_{\eta\eta}\cos\theta\sin\theta+v_{\xi\xi}\sin^2\theta+2v_{\xi\eta}\cos\theta\sin\theta+v_{\eta\eta}\cos^2\theta)]=0$$

Multiplying $\cos\theta$ by the first equation and $\sin\theta$ by the second equation above, after some algebra, we get

$$[\mu(u_{\xi\xi}\cos\theta+v_{\xi\xi}\sin\theta)]=[\mu(u_{\xi\eta}\sin\theta-v_{\xi\eta}\cos\theta)] \tag{2.26}$$

Now we are ready to derive the jump condition for $\partial p/\partial\mathbf{n}$ from the momentum equation in the local co-ordinates

$$[\nabla p\cdot\mathbf{n}]=[\mu(u_{\xi\xi}+u_{\eta\eta})]\cos\theta+[\mu(v_{\xi\xi}+v_{\eta\eta})]\sin\theta=[\mu(u_{\xi\eta}\sin\theta-v_{\xi\eta}\cos\theta)]$$
$$=\frac{\partial^2\gamma}{\partial\mathbf{t}^2}\sin^2\theta-\kappa\frac{\partial\gamma}{\partial\mathbf{t}}\sin\theta\cos\theta+\frac{\partial^2\gamma}{\partial\mathbf{t}^2}\cos^2\theta+\kappa\frac{\partial\gamma}{\partial\mathbf{t}}\sin\theta\cos\theta=\frac{\partial^2\gamma}{\partial\mathbf{t}^2}$$

This completes the proof of Theorem 1.

Remark 1
If we denote

$$\hat{f}_1=\gamma,\qquad \hat{f}_2=\frac{\partial\gamma}{\partial\mathbf{t}} \tag{2.27}$$

as the normal and tangential force strength, then the jump conditions proved in the theorem are the same as those derived in References [18,11] for continuous viscosity.

3. NUMERICAL METHOD

For simplicity, we assume that the domain Ω is a rectangle $[a,b]\times[c,d]$, and the spatial spacing is $h=(b-a)/M=(d-c)/N$, where M and N are the number of grid points in the x- and y-directions respectively. A standard uniform grid is used but the scheme discussed in this section can be generalized to other grids as well without substantial difficulty.

We use a marked particle approach to express the moving interface since we are not particularly interested in topological changes at this stage. The advantages of using the particle approach include: (a) taking advantage of the spline interpolation package developed in [14], which can also find the tangential derivatives easily for a quantity defined on the interface; (b)

better control of accuracy and area preservation since we have control of the number of points on the interface. The main steps used to move the interface from time t^n to t^{n+1} are the following:

- Evaluate the interface information such as the tangential and normal directions, the jumps and their derivatives along the interface using the periodic spline interpolation package [14].
- Use the IIM method [13,14] to solve the Poisson equation for the pressure. With the IIM method, the discrete system of equations is the standard Laplacian plus some correction terms at irregular grid points (those points whose 5-point stencil includes points on both sides of the interface). The cost is just a little more than one call to the fast Poisson solver (which in this paper is the one from Fishpack [19]).
- Interpolate the pressure to get p_x and p_y including those grid points near or on the interface. The standard central finite difference schemes at a regular grid point (x_i, y_j) are

$$p_x = \frac{p_{i+1,j} - p_{i-1,j}}{2h}, \qquad p_y = \frac{p_{i,j+1} - p_{i,j-1}}{2h}$$

  At an irregular grid point, we use the one-sided weighted least square interpolation [16] to get p_x and p_y. For example,

$$p_x(x_i, y_j) = \sum_{k,l} \beta_{kl} p_{kl}$$

  where the summation is taken for those points (x_k, y_l) that are on the same side of the interface as (x_i, y_j) and

$$(x_k - x_i)^2 + (y_l - y_j)^2 \le \delta^2$$

  for a given $\delta \sim Ch$, for some constant C. In our test, C is usually chosen as $3.6h$. Such interpolation gives smooth error distribution and good accuracy. Usually the system of equations for the interpolation coefficients is underdetermined and is solved using the singular value decomposition process. Since the dimension of the system is small, such interpolation does not add much extra cost to the entire algorithm.
- Use the fast IIM method [16] to solve the elliptic equations with the given jump conditions. Since there can be a big jump in the viscosity, such a solution process used to be the most expensive part. In the fast IIM method, we introduce an unknown jump $[u_n]$, which is only defined along the marked particles. A GMRES iteration is used to solve the unknown $[u_n]$. Each iteration of GMRES is one call to the fast Poisson solver. With the fast IIM method, the number of iterations is *independent* of both the jump in the coefficients and the mesh size. The fast IIM method takes advantage of the fast Poisson solver from Fishpack [19]. It is almost impossible to simulate the problem discussed here with a large jump in the viscosity without the fast IIM method. The fast IIM solver for elliptic interface problems with piecewise coefficients is available through the public ftp site at North Carolina State University (ftp.ncsu.edu under the directory of /pub/math/zhilin/package).

- Use the weighted least squares interpolation again to interpolate the velocity field at the marked points to get the velocity $\mathbf{U}_k^n$, $k = 1, 2, \ldots, n_b$.
- Update the cell boundary using the computed velocity

$$\mathbf{X}_k^{n+1} = \mathbf{X}_k^n + \Delta t \mathbf{U}_k^n, \quad k = 1, 2, \ldots, n_b \tag{3.28}$$

The time step for the explicit method is chosen as

$$\Delta t = \frac{h^2}{\max_k |\mathbf{U}_k^n| \max\{\mu^+, \mu^-\}} \tag{3.29}$$

While it is reasonable to use an explicit method for two-dimensional simulation, an implicit method may be needed for three-dimensional problems.

4. NUMERICAL EXAMPLES

All the calculations in this section were performed at North Carolina State University using Sun workstations. Most simulations are done within hours depending on the number of grid points. We use the spline interpolation package developed in [14] to express the interface.

4.1. Example 1

We first test the classic case in which the surface tension γ is a constant. It is well known that the droplet boundary will relax to a circle, its equilibrium state. The initial droplet boundary is:

$$\tau(\theta) = 0.5 + 0.2 \sin(5\theta), \quad 0 \le \theta \le 2\pi \tag{4.30}$$

where $r = \sqrt{x^2 + y^2}$. The computational domain is $[-1, 1] \times [-1, 1]$.

We tested our code for different viscosity ratios and surface tension. The numerical experiments reveal the following two important features. We know intuitively that the larger the surface tension is, the faster the boundary will approach the equilibrium state, a circle with the same area as the original droplet. Another important factor affecting the interface motion is the ratio μ^-/μ^+ of viscosities inside and outside the boundary respectively. The larger this ratio is the faster the motion. In Figure 3, we plot the cell boundary at different times with different surface tensions and viscosity ratio μ^-/μ^+, using an 80×80 grid and $n_b = 80$ marked points on the cell boundary.

- Surface tension: In Figure 3(a) and (b), the surface tension is $\gamma = 0.01$, a small number, and it takes a relatively long time for the cell boundary to converge to or close to its equilibrium state. In Figure 3(c) and (d), the surface tension is $\gamma = 0.1$, and we see that the cell boundary moves much faster than in the first case.

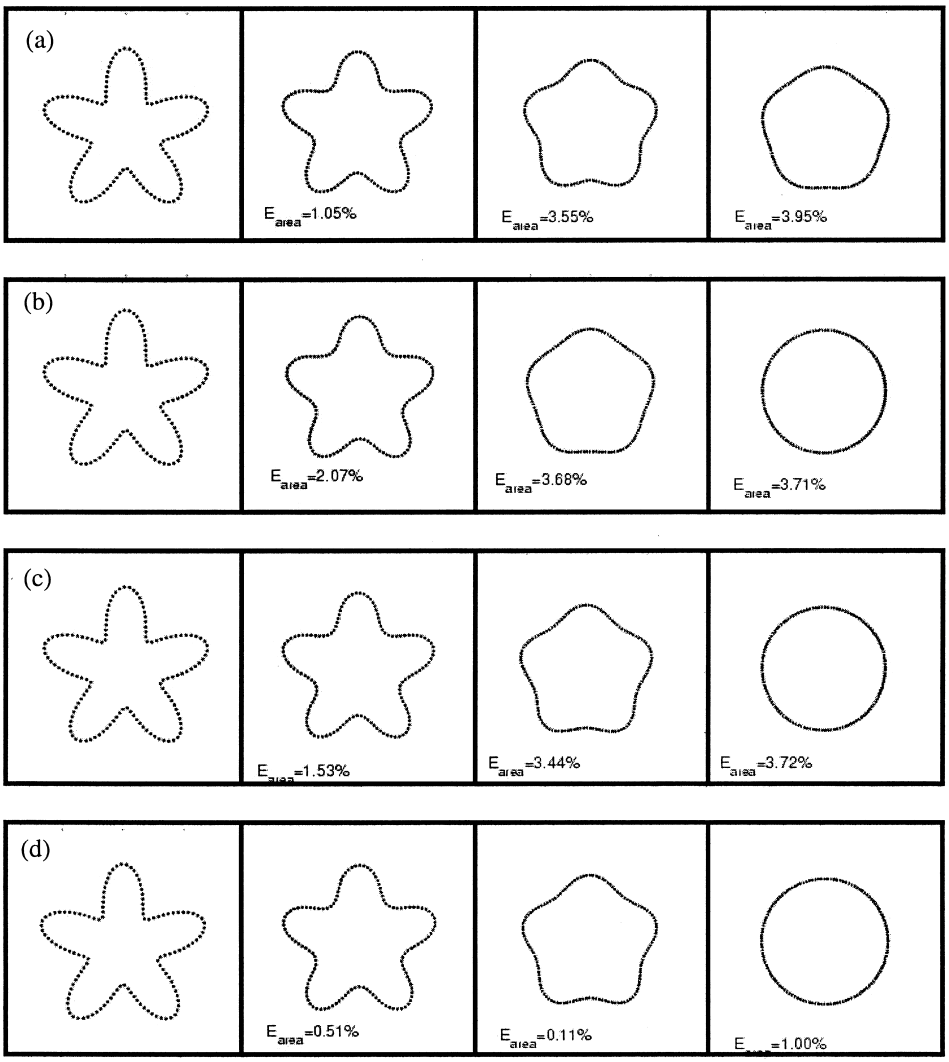

Figure 3. The interface at different times computed using an 80 by 80 grid and a constant surface tension; $\gamma = 0.01$ in (a) and (b), and $\gamma = 0.1$ in (c) and (d). Viscosities are equal ($\mu^- = \mu^+ = 1$) in (a) and (c), and unequal ($\mu^- = 1$, $\mu^+ = 0.01$) in (b) and (d). While the boundary in all cases asymptotically approaches the circular equilibrium state, the time scale is very different. The boundary moves faster as surface tension γ or viscosity ratio μ^-/μ^+ gets larger. (a) Equal viscosity, small surface tension. Times $t = 0$, 39.4531, 109.7656, and 163.28. The shape is far from the equilibrium state even with $t = 163$. (b) Unequal viscosity, small surface tension. Times $t = 0$, 14.5128, 37.9503, and 85.1378. The shape is very close to the equilibrium state at $t = 85$. So the motion is much faster than the case with equal viscosity. (c) Equal viscosity, larger surface tension. Times $t = 0$, 10.6074, 30.1222, and 77.0128. The motion is faster than the case with small surface tension but slower than the case with larger ratio of μ^-/μ^+. (d) Unequal viscosity, large surface tension. Times $t = 0$, 1.0761, 2.9288, and 14.6779. The motion is faster than all three other cases in this figure.

- Viscosity ratio: In Figure 3(a) and (c) the ratio is 1 and we see slower motion compared with (b) and (d), even for the same surface tension.

The algorithm preserves both symmetry and area very well. In all cases, the relative area change is less than 4 per cent. The largest area changes are from the first few steps since the initial interface has relatively large curvature. In the figure, E_{area} is the relative error in the area at that particular time.

4.2. Example 2

In this test, we try to use a variable surface tension to model cell cleavage, after the fashion of Greenspan and others [1,2,6]. However, our model tracks two fluid regions instead of one. First we test a case that is similar to the numerical test in [6] and analyzed in [1,2]. The initial cell boundary is a circle

$$x^2 + y^2 = 0.45^2$$

The surface tension is chosen as

$$\gamma = 0.01 + \epsilon\delta_w(x(s)) \tag{4.31}$$

where $x(s)$ is the x co-ordinates of the cell boundary, and $\delta_w(x)$ is defined as

$$\delta_w(x) = \begin{cases} \dfrac{1}{4w}\,(1 + \cos(\pi x/2w)) & \text{if } |x| < 2w \\ 0 & \text{if } |x| \geq 2w \end{cases} \tag{4.32}$$

the discrete delta function for the immersed boundary method [4]. According to the small-deformation theory of Greenspan [1,2], confirmed by He and Dembo [6], the interface will bend in the middle, which is verified by our numerical example. In Figure 4, we plotted the interface at $t = 0$ and $t = 68.125$ for the case of equal viscosity, and $t = 18.2807$ for the case of different viscosities $\mu^+ = 0.01$ and $\mu^- = 1$ with $\epsilon = 5h$. While the choice of the non-linearity in the surface tension will affect the deformation, our numerical experiments agree with He and Dembo's conclusion [6] that the droplet/cell cannot have a large deformation if (4.31) is used. In fact, for our two-dimensional problem, the boundary will stop moving completely if the local curvature reaches zero, hence cleavage is not possible in this model, since it involves passage through zero on its way to negative curvature. He and Dembo [6] resolve this problem by concluding that there is an extra phoretic force responsible for oil droplet cleavage. We resolve this problem for the case of branching morphogenesis by modeling the effect of oriented collagen bundles as an external force [Lubkin SR, Li Z. Force and deformation on branching rudiments: cleaving between hypotheses (in preparation)].

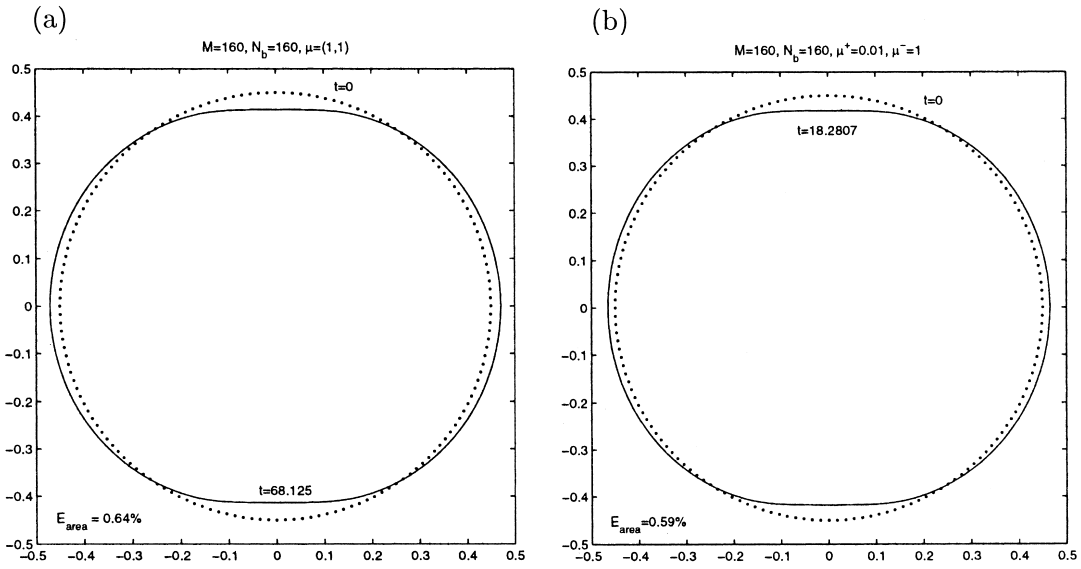

Figure 4. The cell boundary at different times with $\epsilon = 5h$. (a) Equal viscosities $\mu^+ = \mu^- = 1$. (b) Unequal viscosities $\mu^+ = 0.01$ and $\mu^- = 1$. Surface tension given in (4.31). The dotted curve is the initial cell boundary, the circle $r = 0.45$. The solid curve is the cell boundary at (a) $t = 68.125$ and (b) $t = 18.2807$. Again the motion is faster when the ratio μ^-/μ^+ is larger.

4.3. Example 3

In order to have the interface deform further, a different surface tension should be used in the model (1.1)–(1.3). We examined the following surface tension model, corresponding to a localized inwards-directed external force:

$$\gamma = 0.01 - \epsilon\delta_w(x(s)) \tag{4.33}$$

Note that this is similar to the generalized Gibbs–Thomson condition, see Reference [20] and the references therein. The initial interface is the circle $r = 0.45$ with a perturbation

$$r(\theta) = 0.45 + 0.15\cos 2\theta, \quad 0 \le \theta \le 2\pi \tag{4.34}$$

In Figures 5 and 6, we plotted the evolution of the cell boundary with $w = 5h$, and $\epsilon = h$, where $h = (b-a)/M = (d-c)/N$ is the spatial step size, for equal viscosities $\mu^+ = \mu^- = 1$ (Figure 5) and unequal viscosities $\mu^+ = 0.01$ and $\mu^- = 1$ (Figure 6). We see that the area is dividing and eventually will break up. The simulations are done with a 160×160 grid and 160 marked points on the cell boundary. Figures 5(b) and 6(b) are blow-ups of the upper tip. The area conservation errors, marked on the figure, are less than 3.2 per cent, which is relatively

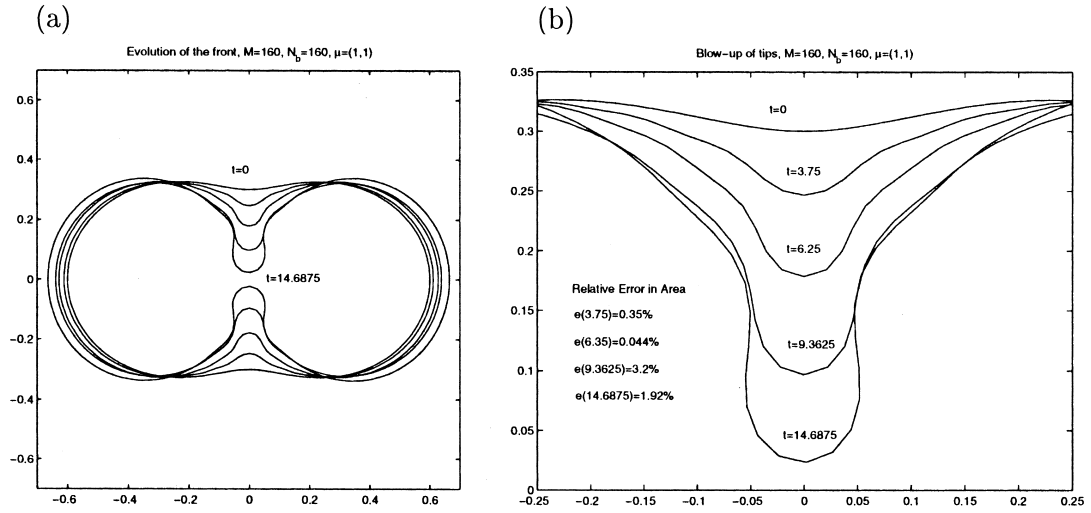

Figure 5. (a) Evaluation of the cell boundary for Example 3 with equal viscosities $\mu^+ = \mu^- = 1$ with $\epsilon = h$. (b) Blow-up of the upper tip. Relative area changes over time are listed in the figure.

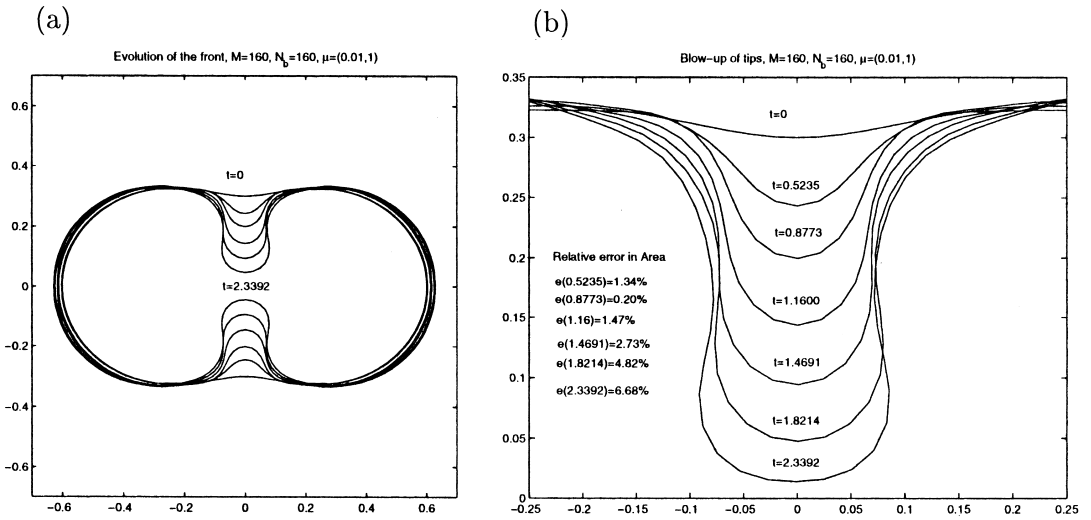

Figure 6. (a) Evolution of the cell boundary for Example 3 with different viscosities $\mu^+ = 0.01$ and $\mu^- = 1$. (b) Blow-up of the upper tip. Relative area changes are listed in the figure. Motion is faster than the case of equal viscosities (Figure 5).

small for such a large deformation. We see similar evolution in both figures but faster motion in the case of unequal viscosities, as discussed for Examples 1 and 2 above.

5. CONCLUSION

We have developed a finite difference method for the Stokes equations for incompressible two-phase flow, which models droplet deformation with discontinuous viscosity and variable surface tension. The decoupled jump conditions for the pressure and the velocity across the interface are crucial for the success of the new algorithm. Our two-dimensional numerical results agree with the results and analysis in the literature for similar choices of the surface tension, in axisymmetric geometry. We took our simulations of a droplet under an external force almost to the point of complete cleavage. While it is known that the motion of a droplet boundary depends on the surface tension, our numerical experiments also demonstrated the dependence of the motion on the difference between the internal and external viscosities.

ACKNOWLEDGMENTS

The first author was partially supported by NSF grant DMS0073403 and ARO grant 39676-MA. The second author was partially supported by NSF grant DMS-9805611. We thank Dr. Xiaobiao Lin for useful discussions.

REFERENCES

1. Greenspan HP. On the deformation of a viscous droplet caused by variable surface tension. *Studies in Applied Mathematics* 1977; **57**: 45–58.
2. Greenspan HP. On the dynamics of cell cleavage. *Journal of Theoretical Biology* 1977; **65**: 79–99.
3. Lister JR. Capillary breakup of a viscous thread surrounded by another viscous fluid. *Physics of Fluids* 1998; **10**: 2758–2764.
4. Peskin CS. Numerical analysis of blood flow in the heart. *Journal of Computational Physics* 1977; **25**: 220–252.
5. Peskin CS, McQueen DM. A general method for the computer simulation of biological systems interacting with fluids. *Symposia of the Society for Experimental Biology* 1995; **49**: 265–379.
6. He X, Dembo M. Numerical simulation of oil-droplet cleavage by surfactant. *Journal of Biomechanical Engineering* 1996; **118**: 201–209.
7. Kang M, Fedkiw R, Liu X.-D. A boundary condition capturing method for multiphase incompressible flow. *Journal of Scientific Computing* 2000; **15**: 323–360.
8. Joseph DD, Renardy YY. *Fundamentals of Two-fluid Dynamics*. Springer: Berlin, 1993.
9. Rallison JM, Acrivos A. A numerical study of the deformation and burst of a viscous drop in an extensional flow. *Journal of Fluid Mechanics* 1978; **89**: 191–200.
10. Stone HA, Leal LG. The effect of surfactants on drop deformation and breakup. *Journal of Fluid Mechanics* 1990; **220**: 161–186.
11. LeVeque RJ, Li Z. Immersed interface method for Stokes flow with elastic boundaries or surface tension. *SIAM Journal of Scientific Computing* 1997; **18**: 709–735.
12. Tu C, Peskin CS. Stability and instability in the computation of flows with moving immersed boundaries: a comparison of three methods. *SIAM Journal of Scientific and Statistical Computing* 1992; **13**: 1361–1376.
13. LeVeque RJ, Li Z. The immersed interface method for elliptic equations with discontinuous coefficients and singular sources. *SIAM Journal of Numerical Analysis* 1994; **31**: 1019–1044.
14. Li Z. The immersed interface method—a numerical approach for partial differential equations with interfaces. PhD thesis, University of Washington, 1994.
15. Li Z. A note on immersed interface methods for three dimensional elliptic equations. *Computers in Mathematic Applications* 1996; **31**: 9–17.

16. Li Z. A fast iterative algorithm for elliptic interface problems. *SIAM Journal of Numerical Analysis* 1998; **35**: 230–254.
17. Li Z, Ito K. Maximum principle preserving schemes for interface problems with discontinuous coefficients. NCSU CRSC-TR00-04, 2000.
18. Lai M-C, Li Z. A remark on jump conditions for the three-dimensional Navier–Stokes equations involving an immersed moving membrane. *Applied Mathematics Letters* 2001; **14**: 149–154.
19. Adams J, Swarztrauber P, Sweet R. Fishpack. http://www.netlib.org/fishback/.
20. Leo PH, Lowengrub JS, Nie Q. Miscrostructural evolution in orthotropic elastic media. *Journal of Computational Physics* 2000; **157**: 44–88.

